Adjustment and Calibration of Dome Port Camera Systems for Underwater Vision

Mengkun She[1,2], Yifan Song[1], Jochen Mohrmann[1], and Kevin Köser[1]

[1] GEOMAR Helmholtz Centre for Ocean Research Kiel, Kiel, Germany
[2] School of Civil Engineering, Chongqing University, Chongqing, China

Abstract. Dome ports act as spherical windows in underwater housings through which a camera can observe objects in the water. As compared to flat glass interfaces, they do not limit the field of view, and they do not cause refraction of light observed by a pinhole camera positioned exactly in the center of the dome. Mechanically adjusting a real lens to this position is a challenging task, in particular for those integrated in deep sea housings. In this contribution a mechanical adjustment procedure based on straight line observations above and below water is proposed that allows for accurate alignments. Additionally, we show a chessboard-based method employing an underwater/above-water image pair to estimate potentially remaining offsets from the dome center to allow refraction correction in photogrammetric applications. Besides providing intuition about the severity of refraction in certain settings, we demonstrate the methods on real data for acrylic and glass domes in the water.

1 Introduction

More than half of Earth's surface is located in the deep ocean. Despite of several decades of underwater photogrammetry (see e.g.[16, 4, 7, 3, 20]), visual mapping of the oceans is by far less developed than from land, air or space, partially because of limited visibility, attenuation and scattering of light as well as the need for more complex observation models due to refraction at the interfaces of camera housings. These housings are required to protect cameras from the surrounding water, and also from the pressure that increases approximately by one bar per ten meter ocean depth. Light rays from objects in the water typically travel through some transparent window into the interior of a housing filled with air surrounding a camera. Because of the different optical densities of water, glass and air, these rays change direction when they pass the interfaces in a non-orthogonal direction (see Fig. 1, left). It has been shown that when using a pinhole camera behind a *flat port*, the overall system becomes a non-single viewpoint camera[23] which makes applications like SLAM and dense reconstruction much more complicated[8, 21]. For instance, the projection of a 3D point into the image requires solution of a twelfth degree polynomial[1]. Additionally, because of strong refraction of outer rays flat ports limit the field of view of the overall system to below 100°. To avoid these limitations spherical glass domes can be used as windows (so-called *dome ports*). In case a camera

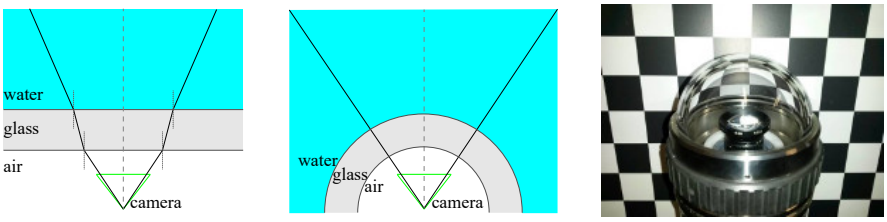

Fig. 1. Left: Incoming light rays are refracted at the flat glass port. Center: If a pinhole camera is positioned at the center of a spheric glass window, a dome port, no refraction occurs because all rays pass the interfaces orthogonal to the surface. Right: Pressure housing with dome port of 5cm radius and 7mm glass thickness for 6000m ocean depth.

is exactly positioned at the center of the dome, all principal rays will pass the air-glass-water interfaces at 90 degrees, avoiding refraction (see Fig. 1, center). However, when the system is not exactly centered (see Fig. 5), non-linear, depth-dependent distortion will occur[10]. Consequently, it is very important to adjust the lens to the dome center and to know the remaining offset in order to allow proper correction of the undesired refraction effects. Finding a lens' nodal point and centering it in the dome is not always an easy task because the dome port might actually only be a fraction of a sphere, rather than a half-sphere, or the center point might be hard to gauge because of the flange construction, in particular for deep sea housings. In this contribution we propose both a mechanical adjustment procedure with visual feedback to align a camera with a dome port as well as a method to estimate a possibly remaining offset. In the next section, our novel contributions will be discussed together with the state of the art in the literature. In Section 3 the mechanical procedure to adjust the lens with the dome is described before Section 4 derives the calibration procedure. In Section 5, we provide detailed evaluation on synthetic ground truth data as well as offset experiments on acrylic domes and a stereo camera system with thick glass domes of a deep sea instrument, before we conclude in Section 6.

2 State of the Art and Contributions

The most common systems for capturing underwater imagery use cameras in underwater pressure housings with either a flat or a dome port. Flat ports are easier to make and therefore typically cheaper. The downside is that cameras behind a flat port will suffer from refraction because of the different media [9], making the overall system a non-single viewpoint camera[23]. This invalidates concepts like the pinhole camera model, including epipolar geometry and common multi-view relations, and complicates robust estimation, outlier detection and bundle adjustment, as for instance projection of a 3D point into the camera requires solution of a high degree polynomial[1]. Besides limited field of view, for deep ocean applications mechanical stability becomes an issue: Here, larger flat windows need to be either of very strong material such as sapphire or have

to be several centimeters thick. The spherical structure of dome ports on the other hand is better suited for higher pressures. The field of view is not limited and pinhole cameras centered in the dome will not suffer from refraction, i.e. photogrammetry and computer vision theory for pinholes in air is applicable. A detailed discussion, also about sharpness and focus issues can be found in [14].

In presence of refraction, camera parameters differ in air and in water[4, 11]. Besides generic ray-based[5] or specialized lookup-table-based representations[12] there are two main mathematical ways of formalizing underwater cameras, either to model and to obtain physical refraction parameters that refer to camera, housing and water[23, 8] or to approximate the underwater camera system, including the housing, by a pinhole camera[20]. In the second concept, when used for flat-port systems, some refraction effects are absorbed into camera parameters such as focal length and radial distortion. Since refraction effects are distance-dependent this concept works best for a predefined, fixed working distance[20] and is problematic in SLAM scenarios where robots see 3D scenes from significantly different distances. Also dome port cameras have been calibrated using pinhole camera calibration techniques[17, 15] assuming a dome-center aligned pinhole. In contrast, in this contribution, we explicitly investigate remaining misalignments and their effects, and follow the concept of modeling and calibrating the physical parameters of the system.

In general, very little work has been published for refraction and calibration with dome ports. The dome port scenario can be split into two subproblems, the mechanical adjustment procedure, to bring a pinhole into the center of a dome port, and the calibration of a potentially remaining offset. The first sub-problem is a similar task as is required in panorama photography, where photographers rotate a camera ideally around its nodal point (the "pinhole") to produce a series of images taken from the same position. Several techniques exist to identify the nodal point of a lens[18], e.g. using a second camera to photograph the iris of the first camera[15], by bringing calibration objects in line[22] and there are even databases for common lenses[19]. The nodal point of the lens and the rotation center of the tripod are typically measured by separate processes, and the camera is mounted in the ad-hoc calculated offset, without a feedback loop for adjustment. Here, it is not obvious how accurately one has to measure the position. For panorama photography of far away landscapes, small errors in the point of rotation are usually neglectable compared to the distance to the scene. In contrast, in photogrammetric underwater applications a millimeter offset can mean substantial refraction errors as will be shown in Fig. 6. Consequently, in this contribution, an adjustment procedure with feedback loop is proposed.

The second subproblem requires identification of the remaining miscalibration. To our knowledge, the only work in the literature that is concerned about this issue is by Kunz and Singh [10], which is the starting point for our work. Unfortunately, the authors motivate the problem only using synthetic data and sketch some ideas about offset computation without reporting results. In contrast, in the remainder of this contribution we will show a new calibration procedure that we evaluate for acrylic and glass domes.

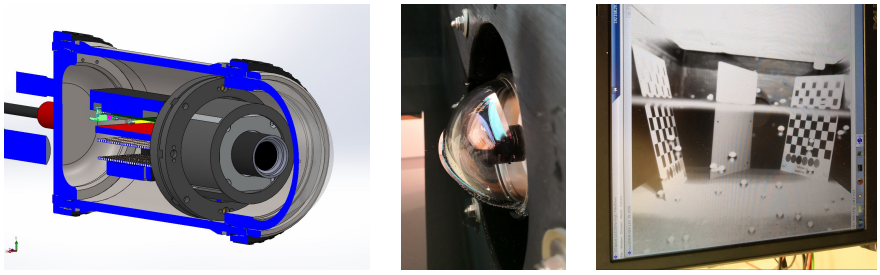

Fig. 2. Left: Technical drawing of deep sea housing with mechanics for camera adjustments towards the dome port. Center: dome port (half underwater) attached to tank. Right: View through dome (after adjustment), with straight lines crossing the surface.

3 Mechanical Adjustment of Cameras

Using the pinhole camera model with underwater dome port cameras requires centering the lens with the dome port as good as possible. The key assumption here is that the lens does not exhibit a caustic in air (see [5]), i.e. it can be considered a pinhole. Within the three possible degrees of freedom (3D offset of the pinhole from dome center), the positioning in camera forward/backward direction poses the largest challenge, as both the lens and the dome port pressure housing are typically rotationally symmetric and their axes can be aligned (already by construction) with high precision. This section proposes a method for mechanically aligning the camera in the difficult forward/backward direction, using the concept of optical feedback control. In principle, this through-the-lens approach allows to adjust the lens, until refraction in this particular camera-lens-dome system becomes neglectable or cannot be observed. Measuring the error in pixels enables also to easily transfer the concept to other lenses that require different spatial alignment accuracy in millimeters without actually having to know that accuracy requirement.

For the mechanical alignment we propose to mount the camera at the flange of the dome port as depicted in Fig. 2 (left). In our design the distance between the camera and the dome can be varied using a screw mechanism (moving 1mm backward/forward per screw rotation). Besides this option, many other constructions are possible where the lens is moved in forward/backward direction while staying centered in the other directions.

Then the dome port should be positioned at a water tank (see Fig. 2, center), such that the dome is half-way underwater and looks parallel to the water surface. In case the camera is centered perfectly, no refraction will occur and the underwater part and the above water part of the image will be consistent. Straight lines that cross the water surface will simply continue. Fig. 3 shows the corresponding images of a chessboard. The task of finding the correct camera position now translates to finding the position at which straight lines in 3D re-

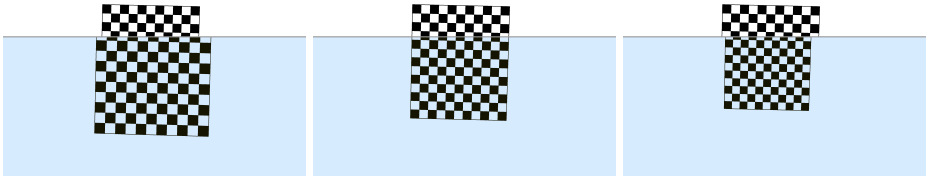

Fig. 3. Simulated Chessboard images with parts above and below the water line. The lens is misaligned forward (left), aligned (center), misaligned backwards (right).

main straight across the water boundary. By manually adjusting the mechanics and viewing the live images, one can determine the correct position easily.

As is well-known in underwater photography (compare also [15]), dome ports change the focus of the camera, because only the principal rays will not be refracted (see Fig. 4). Consequently, different focus or small apertures (large F-numbers) are required to produce an image that is sharp in the underwater part and in the in-air part at the same time. Since the scene is static, small apertures can be compensated by long exposure times. Additionally, if the proposed calibration is performed over larger distances, then the attenuation of light in the water could cause the underwater image part to be much darker than the image part that is in air, which can be alleviated by using underwater lights. Finally, once the straight 3D lines look straight in the camera, we can continue with subpixel offset estimation as outlined in the next section.

4 Calibration of Dome Port Systems

This section describes how to calculate the remaining offsets using an image of a chessboard in air and in water at the same extrinsic settings. It is assumed that the radius, thickness and material of the dome as well as the optical prop-

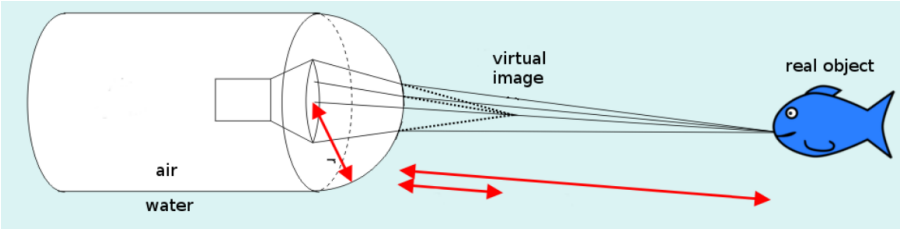

Fig. 4. Focus change induced by dome ports underwater. As can be seen, the principal ray observing the fish is not refracted, but the other rays collected by the lens intersect the dome in a non-orthogonal fashion. This requires setting a much closer focus underwater than in air and poses a challenge for a common lens setting for both.

erties of the water are known. The overall approach consists of five steps: (1) Standard "in-air" perspective camera calibration is performed. (2) The camera is positioned in the dome port and mechanically adjusted to its sphere center by using the method described in Section 3. (3) A chessboard is photographed by the system in air, e.g. in a tank without water. The relative orientation between chessboard and camera is computed by pose estimation. (4) The chessboard (staying at the same relative orientation to the camera) is photographed by the system in water, e.g. the tank is filled. Potential displacements of chessboard corners between the in-air and in-water images are due to refraction induced by the remaining decentering errors. (5) The dome center offset that minimizes the 2D coordinate difference between real measured underwater points and re-projected underwater points (considering refraction) is sought.

4.1 In-air Perspective Calibration

The in-air perspective calibration is a standard camera calibration procedure using calibration targets (e.g. [24]). In the following we will use homogeneous coordinates to formalize the camera model as commonly used (compare [6]): A 3D point is denoted by $\widetilde{\mathbf{P}} = [\mathrm{X}, \mathrm{Y}, \mathrm{Z}, 1]^{\mathrm{T}}$ and its corresponding 2D image position is $\widetilde{\mathbf{p}} = [u, v, 1]^T$. The camera model is formulated as:

$$\widetilde{\mathbf{p}} \simeq \mathbf{K}[\mathbf{R} \mid -\mathbf{RC}]\widetilde{\mathbf{P}} \qquad \text{with} \qquad \mathbf{K} = \begin{bmatrix} f_x & 0 & c_x \\ 0 & f_y & c_y \\ 0 & 0 & 1 \end{bmatrix} \tag{1}$$

where $\mathbf{R}$ and $\mathbf{C}$ are the rotation matrix and camera center that transform from world coordinates to camera coordinates. $\mathbf{K}$ denotes the intrinsic parameters ((f_x, f_y) the focal lengths and (c_x, c_y) the principal point). Additionally, lens distortion parameters can be considered in the perspective camera model as widely used in many calibration tools [2]. However, for the sake of readability, and without loss of generality, in the following derivations we will simply use the matrix $\mathbf{K}$ to account for intrinsic parameters.

4.2 Refractive Back Projection through Dome Ports

In the underwater case, when the camera center is not exactly positioned at the dome port center, incoming light rays are refracted at the outer and inner interfaces of the dome. The refracted ray can be computed from the incident ray and the normal at the refraction surface:

$$\mathbf{r} = \frac{n_i}{n_r}\mathbf{i} + \left(\frac{n_i}{n_r}\cos\theta_i - \sqrt{1 - \sin^2\theta_r}\right)\mathbf{n} \tag{2}$$

where $\mathbf{i}$ and $\mathbf{r}$ are the direction vectors of incident and refracted ray, $\mathbf{n}$ is the normal vector at the intersection point, all those vectors are normalized. n_i and n_r are the indices of refraction for different media. θ_i is the incident angle and

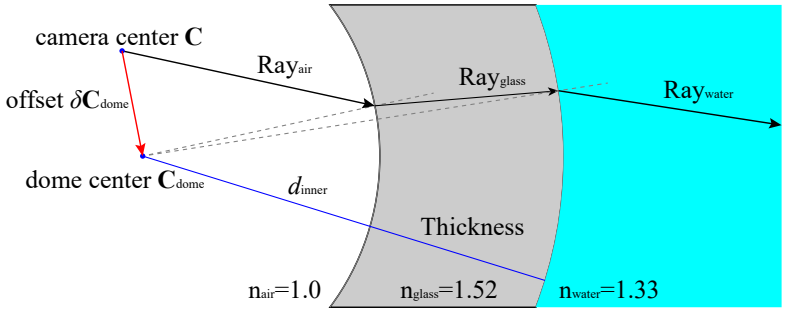

Fig. 5. Refraction of viewing ray in misaligned dome port.

can be calculated by $\theta_i = \arccos(-\mathbf{i} \cdot \mathbf{n})$. θ_r is the refraction angle, which can be derived from the incident angle according to Snell's law $n_i \sin\theta_i = n_r \sin\theta_r$.

In the local camera coordinate system, for a homogeneous 2D point $\widetilde{\mathbf{p}}$ in the underwater image, the viewing ray from the point is determined by

$$\overrightarrow{\mathbf{Ray}}_{air} = \frac{\mathbf{K}^{-1}\widetilde{\mathbf{p}}}{\|\mathbf{K}^{-1}\widetilde{\mathbf{p}}\|_2} \tag{3}$$

If the camera center is set off from the dome center by $\delta\mathbf{C}_{\text{dome}} = (\delta\text{X}_{\text{dome}}, \delta\text{Y}_{\text{dome}}, \delta\text{Z}_{\text{dome}})$, the viewing ray from the image is refracted twice on the air-glass and glass-water interfaces, as shown in Fig. 5. For each refraction, the intersection on the interface is determined by intersecting a ray with a sphere, where spheres can be represented as implicit quadric surfaces[6], e.g. all points $\widetilde{\mathbf{P}}_u$ on the unit sphere fulfill $\widetilde{\mathbf{P}}_u^{\text{T}}\mathbf{Q}\widetilde{\mathbf{P}}_u = 0$ with the unit sphere in diagonal matrix notation $\mathbf{Q} = \text{diag}\{1, 1, 1, -1\}$. The inner and outer spheres of the dome then can be transformed from the unit dome sphere as follows:

$$\mathbf{H}(d, \delta\mathbf{C}_{\text{dome}}) = \begin{bmatrix} d & 0 & 0 & \delta\text{X}_{\text{dome}} \\ 0 & d & 0 & \delta\text{Y}_{\text{dome}} \\ 0 & 0 & d & \delta\text{Z}_{\text{dome}} \\ 0 & 0 & 0 & -1 \end{bmatrix}$$
$$\mathbf{D}(d, \delta\mathbf{C}_{\text{dome}}) = (\mathbf{H}^{-1})^{\text{T}}\mathbf{Q}\mathbf{H}^{-1}, \tag{4}$$

where d indicates the radius of inner and outer sphere of the dome.

The ray-sphere intersection point $\widetilde{\mathbf{P}}_{\text{a/g}}$ on the air-glass interface is satisfying

$$\widetilde{\mathbf{P}}_{\text{a/g}}^{\text{T}}\mathbf{D}_{\text{air}}\widetilde{\mathbf{P}}_{\text{a/g}} = 0 \quad \text{with} \quad \widetilde{\mathbf{P}}_{\text{a/g}} = \lambda_{\text{air}}\overrightarrow{\mathbf{Ray}}_{\text{air}} \tag{5}$$

which boils down to a single quadratic equation in λ_{air}. Once the intersection is determined, the normal vector can be derived and the refracted ray $\overrightarrow{\mathbf{Ray}}_{glass}$ can be calculated by Equation 2. For the glass-water interface, the intersection point $\widetilde{\mathbf{P}}_{\text{g/w}}$ can be calculated in the same way by

$$\widetilde{\mathbf{P}}_{\text{g/w}}^{\text{T}}\mathbf{D}_{\text{glass}}\widetilde{\mathbf{P}}_{\text{g/w}} = 0 \quad \text{with} \quad \widetilde{\mathbf{P}}_{\text{g/w}} = \widetilde{\mathbf{P}}_{\text{a/g}} + \lambda_{\text{glass}}\overrightarrow{\mathbf{Ray}}_{\text{glass}} \tag{6}$$

allowing to compute the outer interface point and ray direction in the water.

4.3 Refractive Projection from 3D Points on a Plane

Since no compact representation of the projection from a 3D point $\mathbf{P}_\mathrm{i}$ into a misaligned dome port camera is known, we use an iterative back-projection approach to implement the projection, similar in spirit to [10]. As we will use it for projecting chessboard corners, the problem can be simplified by working in the chessboard coordinate system, where all 3D points have Z = 0. Essentially, to implement *refractive projection* the euclidean distance between the back-projected 3D point $\hat{\mathbf{P}}_\mathrm{i}$ (according to section 4.2) and the real model point $\mathbf{P}_\mathrm{i}$ is minimized.

$$\mathbf{p}_{\mathrm{i,proj}} = \underset{\mathbf{p}_{\mathrm{i,proj}}}{\operatorname{argmin}} \|\mathbf{P}_\mathrm{i} - \hat{\mathbf{P}}_\mathrm{i}(\mathbf{K}, \mathbf{R}, \mathbf{C}, \delta\mathbf{C}_\mathrm{dome})\|^2 \tag{7}$$

In order to solve this equation, one can project a real model point $\mathbf{P}_\mathrm{i}$ into image space at $\mathbf{p}_\mathrm{i}$ as an initial guess by applying a standard perspective projection. Then a ray from $\mathbf{p}_\mathrm{i}$ is shot back to 3D space according to Section 4.2. Afterwards, the intersection of the double refracted ray and the chessboard plane is computed by finding the point on the ray with Z-component equal to 0, which we consider the back-projected point. The residual is the euclidean distance of these two points, which we minimize using the Gauss-Newton algorithm to obtain the originally sought 2D projection $\mathbf{p}_{\mathrm{i,proj}}$.

4.4 Calibration of Remaining Offsets

To compute the actual 3D offset of a camera from the dome center, an air-water image pair of a chessboard at the same position and orientation is acquired. In case the camera is perfectly centered, the corners in the two images will be exactly at the same location. Displacements indicate that there is refraction due to a centering offset (as the pose stayed the same). Assuming Gaussian noise on the detected chessboard corners, the estimation of the 3D offset $\delta\mathbf{C}_\mathrm{dome}$ can be formulated in the Gauss-Markov model[13], essentially minimizing the energy:

$$E(\delta\mathbf{C}_\mathrm{dome}) = \sum_{\mathrm{i}\in\Omega} \|\mathbf{p}_{\mathrm{i,water}} - \mathbf{p}_{\mathrm{i,proj}}(\mathbf{p}_{\mathrm{i,air}}, \delta\mathbf{C}_\mathrm{dome}, \mathbf{K}, \mathbf{R}, \mathbf{C})\|^2 \tag{8}$$

where $\mathbf{p}_{\mathrm{i,water}}$ and $\mathbf{p}_{\mathrm{i,air}}$ are obtained from the chessboard detection in water and in air separately. $\mathbf{R}$ and $\mathbf{C}$ encode the pose information of the camera relative to the chessboard which can be extracted from the set of in-air 3D-2D correspondences (standard pose estimation). $\mathbf{p}_{\mathrm{i,proj}}$ is the projection of the chessboard point $\mathbf{P}_\mathrm{i}$ through the dome port in the underwater case.

As an initial hypothesis for optimization, zero offset can be assumed, for which the projection yields to the in-air corner positions. We obtain the parameters according to Gauss-Newton optimization in the Gauss-Markov model as outlined in [13, section 2]. The derivatives can be computed by finite differences approximation.

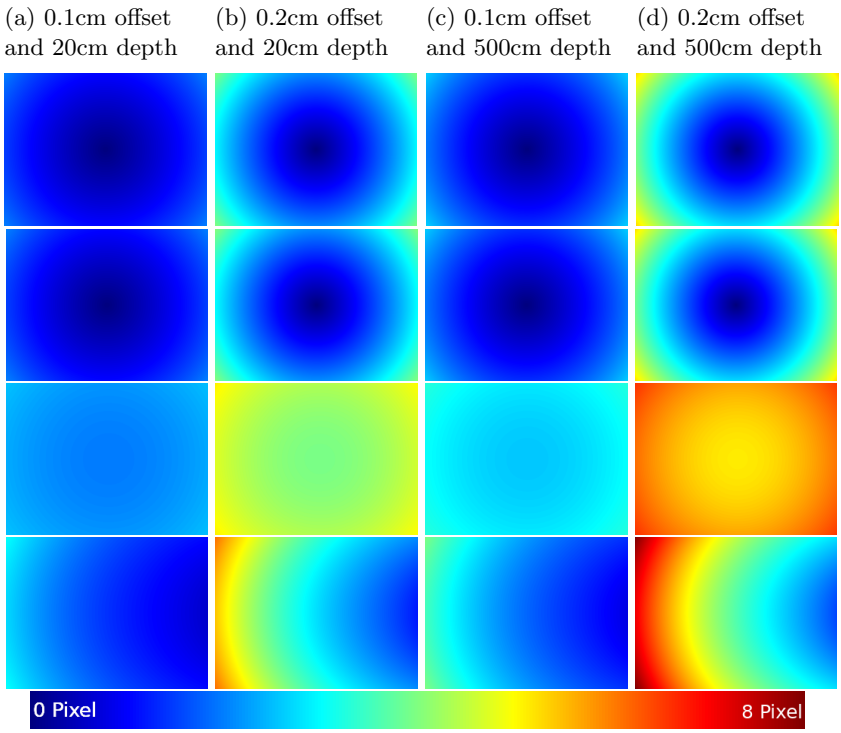

Fig. 6. Magnitude of simulated pixel distortions for different offsets between camera and dome port center. The Pixel are projected from a sphere around the dome port with different depths. From top to bottom: Offset directions forward along the principal axis, backwards along principal axis, orthogonal to principal axis and along a combined direction forward and orthogonal to principal axis (displacement enlarged by $\sqrt{2}$).

5 Evaluation

In order to obtain better insights into the observable magnitudes of refraction, first synthetic ground truth experiments are performed that resemble the parameters of our real 50mm dome port for close range photogrammetry (20cm) or mapping from a distance (5m). The virtual camera was placed at positions with different offsets to the dome center. 3D points on the plane were projected to the image space by using standard perspective projection and dome port refractive projection. The magnitude of pixel displacement between different projections are visualized in Fig. 6.

Simulated Data To validate the offset estimation algorithm, 3D chessboard coordinates with square size 20cm $\times$ 20cm were simulated, taken by a camera with image resolution of 1280×1024, focal length $f_x = f_y = 1700$ and principal point $c_x = 640.5$, $c_y = 512.5$. The dome port was simulated with radius of 50mm and thickness of 7mm. The chessboard corners were projected onto the image plane

using standard perspective projection and refractive dome port projection, in order to generate in-air and in-water "image pairs". Afterwards, Gaussian noise with different noise level was added to the simulated points in the images.

In this experiment, the camera was simulated at different positions with respect to the dome port: $\delta_1 = (0.01, 0.01, 0.01)$, $\delta_2 = (0.002, 0.003, 0.004)$. The noise level σ varies from 0.1 pixels to 0.5 pixels, we performed 50 trials on each position and each noise level. The average absolute value of the relative error is measured between estimated parameters and ground truth. As it is shown in Fig. 7, δ_x and δ_y always give better estimates than δ_z. The main reason is that the offset along the principal axis has less effect on the image displacement compared to the side directions.

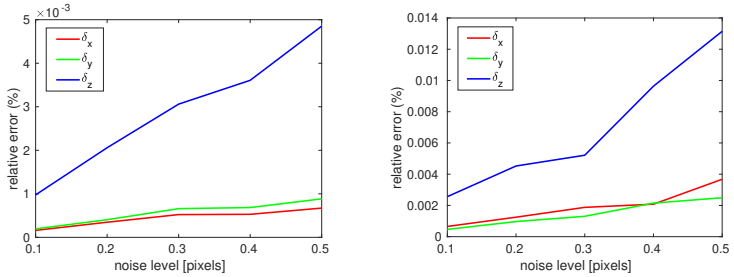

Fig. 7. Error of estimated offset parameters for different Gaussian noise levels. Left:simulated camera at offset $\delta_1 = (0.01, 0.01, 0.01)$ with respect to dome port. Right:simulated camera at offset $\delta_2 = (0.002, 0.003, 0.004)$.

Calibration Validation using an Acrylic Dome The proposed method was then examined on real data. This experiment aims to verify the calculation of offsets between camera and dome center. The setup consists of a low cost webcam within an acrylic dome, which has a radius of 77.45mm and thickness of 2.4mm.

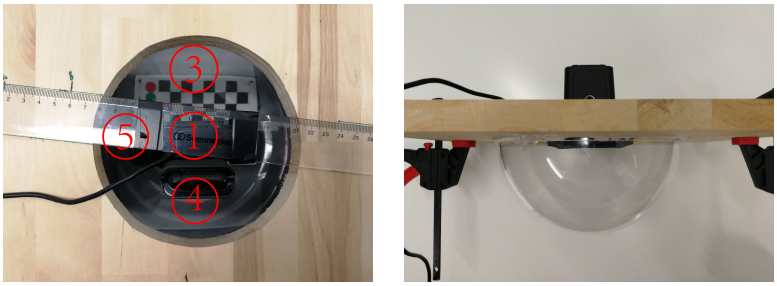

Fig. 8. Experimental settings of the webcam with an acrylic dome. Left: Top view with test positions, Right: Side view.

The in-air calibration of the webcam was performed using a standard toolbox [2]. During the experiments, the webcam was placed at different positions in the dome port (see Fig. 8), which are described in terms of the initial position close to ① the center of the dome port: ② offset 15mm along Z-axis, ③ offset 15mm along Y-axis, ④ offset -15mm along Y-axis, ⑤ offset 20mm along X-axis.

The calibration results are shown in Table 1.

.

Table 1. Calibration results of the low cost webcam with acrylic dome ports

	offsets			residual[pixel]	
	δ_x[mm]	δ_y[mm]	δ_z[mm]	before calibration	after calibration
Test ①	0.8071	3.3953	1.8441	5.6855	0.8051
Test ②	1.5459	4.5547	15.7268	7.8347	0.6356
Test ③	-0.6054	17.6406	-0.7525	30.1930	1.6123
Test ④	1.1253	-11.7163	5.2843	19.2762	0.8741
Test ⑤	-14.3336	0.3173	0.1010	23.8291	0.5925

The experiment shows that the proposed calibration algorithm provides reasonable offset values. When using the computed offsets, the residuals of the re-projection error are significantly improved and the computed offsets agree very well with the physically measured offsets. Remaining differences can be explained by the inaccurate experiment setup and the imperfection of the cheap acrylic dome which is not an optical instrument .

Deep Sea Glass Dome Stereo System The proposed technique has also been applied to a stereo camera system (two Basler cameras with 1280×1024 resolution) with high quality glass domes (radius 50.10mm and thickness 7mm). The cameras were first mechanically adjusted according to the proposed approach of Section 3. The result of the mechanical adjustment procedure can be seen in Fig. 2(right), the calibration and evaluation results are shown in the Table 2.

Table 2. Calibration results of the stereo cameras with glass dome ports.

	offsets			residual[pixel]	
	δ_x[mm]	δ_y[mm]	δ_z[mm]	before calibration	after calibration
Master Camera	0.0490	0.5033	-0.2967	2.9552	0.2847
Slave Camera	-0.2431	0.0012	0.0324	6.5177	0.4120

As it can be seen, the mechanical adjustment is able to align the camera center to the dome center in sub-millimeter accuracy.

As a second evaluation the stereo system is calibrated in air, and submerged into water. Then we plot the epipolar lines of some chessboard corners from

left image to right image (see Fig. 9 left). Using the in-air calibration there are significant errors in the epipolar lines. Using the calibration of the offset of the dome port, the epipolar lines cross the corresponding chessboard corners in the right image almost perfectly (see Fig. 9 right), which demonstrates that the offset calibration is useful.

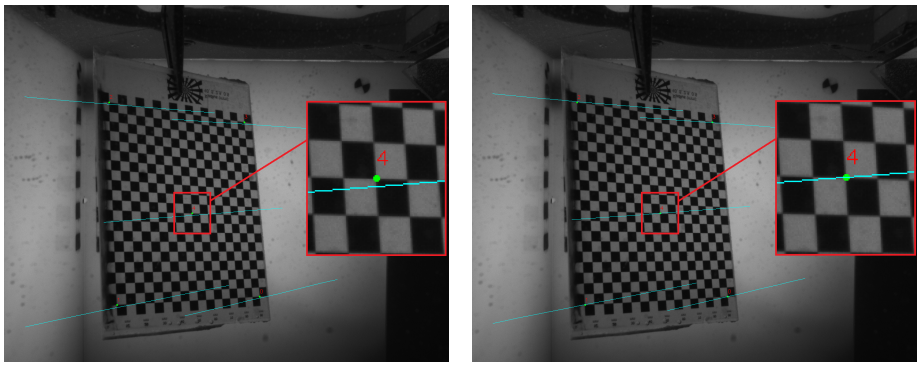

Fig. 9. Epipolar lines of chessboard corners from right camera plotted in left camera image. Left: before offset calibration, Right: after offset calibration.

6 Conclusion

To avoid refraction and to allow for using the pinhole camera model and well-known multiple view relations, dome ports can be used for underwater vision. However, it is important to position the camera exactly at the center of the dome, which is not an easy task because the dome port might actually only be a fraction of a sphere, rather than a half-sphere, or the center point might be hard to gauge because of the flange of the pressure housing, in particular for deep sea housings. At the same time, the nodal point of the camera cannot be seen easily and has to be measured in any case.

In this contribution we have shown a method with visual feedback to mechanically align the camera with the center of an optical dome port and have proven that we can achieve sub-millimeter accuracy using the method. Additionally, we have presented a new calibration algorithm based on an air-water image pair of a chessboard in order to estimate the remaining refraction effects. Using the calibration information, residual errors can be improved and epipolar geometry can be made much more consistent. The result can therefore be used as a correction term in photogrammetric measurements or could also be used to further improve the mechanical adjustment. On top of these new methods, we have also presented sensitivity analyses to provide intuition about expectable refraction given inaccurate alignments. Future work should integrate these findings into an underwater camera calibration toolbox.

Acknowledgements

The authors would like to thank Matthias Wieck for designing and manufacturing the mechanical alignment mount for the dome port camera system and Dr. Anne Jordt for sharing refraction source code. This publication has been cofunded by the German Research Foundation (Deutsche Forschungsgemeinschaft, DFG) Projektnummer 396311425, through the Emmy Noether Programme. This publication also been cofunded by the European Unions Horizon 2020 research and innovation programme under grant agreement No. 690416-H2020-SC5-2015-one-stage (ROBUST). The authors of this paper are also grateful for support from the Chinese Scholarship Council (CSC) for Yifan Song.

References

1. Agrawal, A., Ramalingam, S., Taguchi, Y., Chari, V.: A theory of multi-layer flat refractive geometry. In: CVPR (2012)
2. Bouguet, J.: Camera calibration toolbox for matlab. http://www.vision.caltech.edu/bouguetj/calib_doc/index.html, accessed 2019-05-19
3. Drap, P.: Underwater photogrammetry for archaeology. In: da Silva, D.C. (ed.) Special Applications of Photogrammetry, chap. 6. IntechOpen, Rijeka (2012). https://doi.org/10.5772/33999, https://doi.org/10.5772/33999
4. Fryer, J.G., Fraser, C.S.: On the calibration of underwater cameras. The Photogrammetric Record **12**, 73–85 (1986)
5. Grossberg, M.D., Nayar, S.K.: The raxel imaging model and ray-based calibration. International Journal of Computer Vision **61**(2), 119–137 (2005)
6. Hartley, R., Zisserman, A.: Multiple View Geometry in Computer Vision (Second Edition). Cambridge University Press, second edn. (2004)
7. Harvey, E.S., Shortis, M.R.: Calibration stability of an underwater stereo-video system : Implications for measurement accuracy and precision. Marine Technology Society journal **32**, 3–17 (1998)
8. Jordt, A., Köser, K., Koch, R.: Refractive 3d reconstruction on underwater images. Methods in Oceanography **15-16**, 90 – 113 (2016). https://doi.org/https://doi.org/10.1016/j.mio.2016.03.001, http://www.sciencedirect.com/science/article/pii/S2211122015300086
9. Kotowski, R.: Phototriangulation in multi-media photogrammetry. Intl Archives of Photogrammetry and Remote Sensing **XXVII** (1988)
10. Kunz, C., Singh, H.: Hemispherical refraction and camera calibration in underwater vision. In: OCEANS 2008. pp. 1–7 (15-18 2008). https://doi.org/10.1109/OCEANS.2008.5151967
11. Lavest, J.M., Rives, G., Lapresté, J.T.: Underwater camera calibration. In: ECCV '00: Proceedings of the 6th European Conference on Computer Vision-Part II. pp. 654–668 (2000)
12. Luczynski, T., Pfingsthorn, M., Birk, A.: The pinax-model for accurate and efficient refraction correction of underwater cameras in flat-pane housings. Ocean Engineering **133**, 9 – 22 (2017). https://doi.org/https://doi.org/10.1016/j.oceaneng.2017.01.029, http://www.sciencedirect.com/science/article/pii/S0029801817300434
13. McGlone, J.C. (ed.): Manual of Photogrammetry. ASPRS, 5th edn. (2004)

14. Menna, F., Nocerino, E., Remondino, F.: Optical aberrations in underwater photogrammetry with flat and hemispherical dome ports. vol. 10332 (2017). https://doi.org/10.1117/12.2270765, https://doi.org/10.1117/12.2270765
15. Menna, F., Nocerino, E., Fassi, F., Remondino, F.: Geometric and optic characterization of a hemispherical dome port for underwater photogrammetry. Sensors **16**(1) (2016). https://doi.org/10.3390/s16010048, http://www.mdpi.com/1424-8220/16/1/48
16. Moore, E.J.: Underwater photogrammetry. The Photogrammetric Record **8**(48), 748–763 (1976). https://doi.org/10.1111/j.1477-9730.1976.tb00852.x, https://onlinelibrary.wiley.com/doi/abs/10.1111/j.1477-9730.1976.tb00852.x
17. Nocerino, E., Menna, F., Fassi, F., Remondino, F.: Underwater Calibration of Dome Port Pressure Housings. ISPRS - International Archives of the Photogrammetry, Remote Sensing and Spatial Information Sciences pp. 127–134 (Mar 2016). https://doi.org/10.5194/isprs-archives-XL-3-W4-127-2016
18. PanoramicPhotoGuide: Finding the nodal point. https://panoramic-photo-guide.com/finding-the-nodal-point.html, accessed 2019-05-19
19. PanoTools.org: Entrance pupil database. https://wiki.panotools.org/Entrance_Pupil_Database, accessed 2019-05-19
20. Shortis, M.: Calibration techniques for accurate measurements by underwater camera systems. Sensors **15**(12), 30810–30826 (2015). https://doi.org/10.3390/s151229831, http://www.mdpi.com/1424-8220/15/12/29831
21. Song, Y., Köser, K., Kwasnitschka, T., Koch, R.: Iterative refinement for underwater 3d reconstruction: Application to disposed underwater munitions in the baltic sea. ISPRS - International Archives of the Photogrammetry, Remote Sensing and Spatial Information Sciences **XLII-2/W10**, 181–187 (2019). https://doi.org/10.5194/isprs-archives-XLII-2-W10-181-2019, https://www.int-arch-photogramm-remote-sens-spatial-inf-sci.net/XLII-2-W10/181/2019/
22. TheDigitalPicture: How to find the nodal point for your lens. https://the-digital-picture.com/News/News-Post.aspx?News=27452, accessed 2019-05-19
23. Treibitz, T., Schechner, Y., Kunz, C., Singh, H.: Flat refractive geometry. IEEE Transactions on Pattern Analysis and Machine Intelligence **34**(1), 51–65 (Jan 2012). https://doi.org/10.1109/TPAMI.2011.105
24. Zhang, Z.: Flexible camera calibration by viewing a plane from unknown orientations. In: Proceedings of the International Conference on Computer Vision. pp. 666–673. Corfu, Greece (1999), http://www.citeulike.org/user/snsinha/article/238276